

Multi-UAV trajectory planning for 3D visual inspection of complex structures

Stefan Ivić^a, Bojan Crnković^b, Luka Grbčić^{a,d}, Lea Matleković^c

^aFaculty of Engineering, University of Rijeka, Vukovarska 58, Rijeka, 51000, Croatia

^bDepartment of Mathematics, University of Rijeka, Slavka Krautzeka 75, Rijeka, 51000, Croatia

^cDepartment of Mathematics and Computer Science, University of Southern Denmark, Campusvej 55, Odense, 5230, Denmark

^dCenter for Advanced Computing and Modelling, University of Rijeka, Radmile Matejčić 52, Rijeka, 51000, Croatia

Abstract

This paper presents a new trajectory planning algorithm for three-dimensional autonomous UAV volume coverage and visual inspection. The algorithm is an extension of a state-of-the-art Heat Equation Driven Area Coverage (HEDAC) multi-agent area coverage algorithm for three-dimensional domains. With a given target exploration density field, the algorithm designs a potential field to achieve the minimization of the remaining density and generate trajectories using potential gradients to direct UAVs to the regions of higher potential, i.e., higher values of remaining density. Collisions between the agents and agents with domain boundaries are prevented by implementing the distance field and correcting the agent's directional vector when the distance threshold is reached. A unit cube test case is considered to evaluate this trajectory planning strategy for volume coverage. The case demonstrates successful collision avoidance even inside a crowded domain with a hundred UAVs exploring it. For visual inspection applications, the algorithm is supplemented with camera direction control. A field containing the nearest distance from any point in the domain to the structure surface is designed. The gradient of this field is calculated to obtain the camera orientation throughout the trajectory. Three different test cases of varying complexities are considered to validate the proposed method for visual inspection. The simplest scenario is a synthetic portal-like structure inspected using three UAVs. The other two inspection scenarios are based on realistic structures where UAVs are commonly utilized: a wind turbine and a bridge. When deployed to a wind turbine inspection, two simulated UAVs traversing smooth spiral trajectories have successfully explored the entire turbine structure while cameras are directed to the curved surfaces of the turbine's blades. In the bridge test case, commonly used as a test case in scientific publications focused on UAV inspection, an efficacious visual inspection of a complex structure is demonstrated by employing a single UAV and five UAVs. The proposed methodology is successful in planning the UAV visual inspection. It offers flexibility in various setup parameters and is applicable in real-world inspection tasks.

Keywords: autonomous UAVs, trajectory planning, 3D domain, exploration, coverage, inspection

1. Introduction

In recent years and with the constant demand for automatization of processes, there has been a rising interest in research of autonomous Unmanned Aerial Vehicles (UAVs) and autonomous robotic systems in general. Known for their versatile movements and ability to explore the unstructured environment, UAVs are being employed for numerous civil applications such as transportation [1, 2], monitoring and surveying [3, 4], search and rescue [5, 6] as well as infrastructure inspection [7] intending to increase safety and reduce costs. Tackling the challenge of making a UAV an autonomous agent requires an interdisciplinary approach, collaboration, and knowledge distribution across the fields. The agent must be equipped with accurate sensor technologies enabling the control system to direct the vehicle according to the developed path planning or trajectory planning strategy. Path planning algorithms generate geometric properties of a path, from an initial to a final point, passing through pre-defined via-points, while trajectory planning algorithms take these properties and endow them with time information. In most cases, path planning precedes trajectory planning; however, these two phases are not necessarily

distinct [8]. Path planning and trajectory planning problems are crucial to solve for achieving autonomous flight, imposing additional complexity as the approach usually differs depending on the specific application. When multiple UAVs are involved, planning algorithms should consider collision avoidance between agents and optimization of their interactions. Although more complex, multi-agent path or trajectory planning naturally achieves flight mission objectives faster and with high precision, making it an attractive research topic.

The focus of this paper is on trajectory planning for volume exploration and coverage. The problem is very similar to the Coverage Path Planning (CPP) problem which aims at determining a path that passes through all points of an area or volume of interest while avoiding obstacles [9]. Additionally, trajectory planning generates feasible trajectories according to vehicle kinematics and environmental constraints, making it more suitable for real-life applications. CPP algorithms are often developed for the reconstruction of the environment and creation of the digital models. Categorization of approaches into model-based and non-model-based is presented in [10]. Model-based approaches use the reference model of the area or structure

of interest to generate a path that encapsulates a set of viewpoints providing the maximum coverage for reconstruction and mapping. The non-model-based approaches do not use a priori knowledge of the environment, therefore require online iterative calculations for choosing and evaluating candidate viewpoints producing the path with maximum coverage.

Two-dimensional coverage path planning for area reconstruction and exploration are very well researched topics [11]. Having a knowledge of the flight environment, some CPP model-based approaches are also employed for volume exploration and infrastructure inspection. Most of these approaches plan waypoints around the structure of interest and afterward either generate trajectories between waypoints or employ a point-to-point flight controller. Some drawbacks of these approaches are that algorithms are not easily adaptable for different structural models and, when flying point-to-point, the controller affects the precision of path execution. As UAVs are limited in energy and computational power, CPP approaches require computationally efficient and robust path calculation producing feasible trajectories by taking into account environmental and vehicle constraints to accomplish the autonomous mission's objective. These requirements impose an ongoing challenge in the research community, especially for the inspection of three-dimensional structures.

Within this work, we address the challenge by proposing a new, robust coverage trajectory planning algorithm for three-dimensional volume exploration and structural inspection using multiple flying agents with the ability to set the desired coverage density taking into account the vehicle kinematics and environmental constraints. The trajectory planning algorithm is based on a potential field approach, designing the field using HEDAC (Heat Equation Driven Area Coverage) algorithm [12] which minimizes the difference between the desired and achieved coverage, therefore, leading the agents through uncovered locations. We validate the algorithm on several examples which include a synthetic example and two realistic cases with varying structural complexity.

This article is organized as follows. Section 2 presents an overview of the state-of-the-art research concerning three-dimensional coverage path planning and trajectory planning as well as the HEDAC algorithm foundation and applications to two-dimensional coverage problems. In Section 3, the adaptation of the HEDAC algorithm for three-dimensional domains is presented with the first implementation, based on the finite element method (FEM), to a 3D unit cube ergodic exploration example. In Section 4, we adapt the algorithm for 3D visual inspection by introducing the distance field and the camera orientation. We present the simulation results for the HEDAC UAV inspection of a portal, wind turbine, and bridge structures. Finally, in Section 6, we conclude by stating the achievements and limitations of the presented methodology.

2. State-of-the-art

Exploration and coverage path planning for mobile agents are current challenges in the field of autonomous robotic systems. Well researched scenarios deal with path planning and

trajectory planning for two-dimensional areas employing algorithms like Spectral Multiscale Coverage (SMC), Receding Horizon Control (RHC), Lawnmower, or Heat Equation Driven Area Coverage (HEDAC). The focus of this article is on the HEDAC algorithm adaptation for three-dimensional exploration and coverage trajectory planning for visual inspection. Therefore, this section provides an overview of the existing HEDAC research based on two-dimensional applications and presents current state-of-the-art methods for three-dimensional volume exploration and coverage path planning based on the number of agents. By conducting an extensive literature review, we analyzed existing algorithms applied to visual inspection. Most of the solutions were either limited in the number of agents conducting the inspection or provided a geometric path calculation for the selected infrastructure model, excluding flight trajectories.

2.1. HEDAC multi-agent trajectory planning

An ergodic multi-agent area coverage method based on a potential field approach is presented in [12]. Heat Equation Driven Area Coverage (HEDAC) algorithm designs a potential field based on a steady-state heat equation using a source term that depends on the difference between the given goal density distribution and the current coverage density. The agents' movements are directed by the gradient of that potential field, leading them to the area of interest and producing paths to achieve the goal coverage density while avoiding collisions between agents using a built-in local cooling mechanism. The execution of the algorithm is demonstrated on three 2D area coverage test cases and compared with the Spectral Multiscale Coverage (SMC) algorithm showing superiority in achieved coverage and computational time.

The HEDAC algorithm application to autonomous non-uniform multi-agent spraying is presented in [13]. The algorithm combines the spraying model and Dubins motion model to produce the path covering the spraying area with the goal density. The method was tested in comparison with Lawnmower and SMC algorithms for simple geometries as well as a realistic crop spraying case, outperforming both methods in convergence time while producing spraying density of satisfying accuracy and using less spraying media when compared with conventional spraying.

Adaptation of HEDAC algorithm for multi-agent area search in uncertain conditions is presented in [14]. The undetected target probability-density field is computed from the initial probability field, already achieved agents' trajectories, and diverse motion and sensing parameters of each agent. The HEDAC method directs agents toward regions with a higher concentration of undetected targets resulting in the maximization of the target detection rate. The target search using HEDAC was simulated and compared with Lawnmower, SMC, and Receding Horizon Control (RHC) approaches, demonstrating a shorter search time for a given number of targets.

Improvement of the HEDAC algorithm for multi-agent surveying constrained motion control in irregular domains is proposed in [15]. The previous implementation considered rectangular domains due to using the finite difference method for

solving a partial differential equation regulating the potential. The improved solution uses the finite element method to enable a simple and elegant application of boundary conditions and modeling static obstacles in the domain. Optimization for collision avoidance maneuvers and the ability to set the path curvature constraints improved the HEDAC algorithm’s suitability for real-world 2D area surveying applications. The algorithm was tested in a synthetic scenario as well as two realistic scenarios providing results with high computational efficiency with the possibility of real-time execution.

2.2. Single-agent coverage path planning

A Co-optimal Coverage Path Planning (CCPP) method that simultaneously co-optimizes the UAV path, quality of the captured images, and reduces the computational complexity of the solver all while adhering to safety and inspection requirements is presented in [16]. The path optimization algorithm utilizes a Particle Swarm Optimization (PSO) framework which iteratively optimizes the coverage paths without needing to discretize the motion space or simplify the sensing. The core of the method consists of a cost function that measures the quality and efficiency of a coverage inspection path and the greedy heuristic for the optimization enhancement by aggressively exploring the viewpoints search spaces.

Based on the 3D model, the authors in [17] proposed a coverage path planning algorithm for the inspection of planar surfaces, taking into account obstacle avoidance. Inspection viewpoints are generated based on a grid decomposition and an enhanced Discrete Particle Swarm Optimization (DPSO) algorithm is then used to solve the Traveling Salesman Problem (TSP) with performance improvement by using deterministic initialization, random mutation, and edge exchange. Taking advantage of parallel computing, DPSO was implemented in a GPU-based framework so that the computation time can be significantly reduced while keeping the hardware requirement unchanged. The authors proposed to improve path planning by extending the algorithm for non-planar surfaces and incorporating online replanning for irregular shapes inspection.

A multi-resolution hierarchical framework method for solving coverage planning is proposed in [18]. The authors’ sample camera viewpoints in the overall environment based on a priori-known map. After sampling all viewpoints, a collision check is run to eliminate the viewpoints colliding with structures in the environment. Paths are computed at two different levels. Firstly, a high-level algorithm separates the environment into multiple subspaces at different resolutions and solves the global TSP to compute an order of the subspaces for traversal. Secondly, a low-level sampling-based algorithm solves for paths within the subspaces for detailed coverage resolving collisions by adding new viewpoints. The resulting method runs significantly faster than other state-of-the-art methods.

A path planning method based on the point cloud generated from a 3D model, representing complex inspection targets, is presented in [19]. The method is designed as a sampling-based sequential optimization to calculate and optimize an inspection path while considering the limitation of the sensors, inspection efficiency, and safety requirements of the UAVs. A voxel

downsampling method is employed to uniformly sample the point cloud, and a bounding box is created around the points. Flight waypoints are generated by projecting the points onto the planes of the bounding box. A traversal path search algorithm is proposed to find paths through the waypoints. The proposed method is evaluated for use cases of bridge and power pylon inspection. A comparison between the proposed traversal path search algorithm and the basic greedy TSP solver [20] is made where the proposed algorithm found simpler paths in less time.

A similar approach for coverage path planning based on a priori-known volumetric map is presented in [21], resulting in high infrastructure coverage and reduced computation time. The 3D structure is divided into several layers, and in each layer, a set of normal vectors of each voxel’s center point is calculated. The opposing vectors are used as viewpoints, downsampled with a voxel grid filter. Then, the shortest tour connecting the viewpoints is computed with the Lin–Kernighan Heuristic (LKH) TSP solver, and all paths in each layer are combined to form a complete path.

A new path planning algorithm for autonomous robotic exploration and inspection is presented in [22]. The proposed method plans online in a receding horizon fashion by sampling possible future configurations in a geometric random tree. The choice of the objective function enables the planning for either the exploration of unknown volume or inspection of a given surface manifold in both known and unknown volume. The presented analysis of computational complexity and thorough simulation-based evaluation indicate good scaling properties with respect to the scenario complexity. Feasibility and practical applicability are demonstrated in real-life experimental test cases with full on-board computation.

The authors in [23] proposed the inspection path planning approach for complex 3D structures based on a triangular mesh representation. The approach computes short inspection paths via an alternating two-step optimization algorithm which at every iteration attempts to find a new and improved set of viewpoints that together provide full coverage with decreased path cost. The algorithm supports the integration of multiple sensors with different fields of view, the limitations of which are respected. Both fixed-wing, as well as rotorcraft aerial robot configurations, are supported and their motion constraints are respected at all optimization steps, while the algorithm operates on both mesh and occupancy map-based representations of the environment. The authors thoroughly evaluated the approach using the radio/tv tower and trolley models extending their work in [24] by planning the coverage path for the wind turbine, staircase, mountain, and cone models.

To find an efficient flight path for a UAV for visually inspecting a transmission tower, authors in [25] formulated an optimization model. The objective of the model is to maximize a function involving three performance ratios, namely, flight time, image quality, and tower coverage. The optimization model is non-linear, non-differentiable, and multi-modal. The problem is solved by using a Particle Swarm Optimization (PSO) based algorithm and a Simulated Annealing (SA) based algorithm. The experimental results showed that the PSO-based algorithm outperformed the SA-based algorithm.

2.3. Multi-agent coverage path planning

A Cooperative Coverage Path Planning (C-CPP) for the inspection of complex infrastructures by utilizing multiple Unmanned Autonomous Vehicles (UAVs) is presented in [26]. The proposed scheme is able to generate multiple paths for UAVs in order to achieve complete cooperative coverage. Initially, the infrastructure under inspection is being sliced by horizontal planes, which has the capability of recognizing the branches of the structure. These branches are handled as breaking points for the path planning of the UAVs to collaboratively execute the coverage task in less time and more realistically, based on the current flying times of the UAVs. Flight waypoints are generated based on the horizontally sliced 3D model and converted into position-velocity-yaw trajectories, which can be directly provided to the linear model predictive controller cascaded over an attitude-thrust controller. To guarantee the overall flight safety in unpredictable or faulty situations, the authors employed an online avoidance scheme.

A methodology for three-dimensional area coverage using multiple small UAVs based upon a customized cell decomposition algorithm is presented in [27]. The algorithm divides a polygon, selected on a 3D elevation map, into regular hexagons and allocates UAVs to hexagons. The lawnmower coverage pattern is generated by using vertical segmentation of the hexagons to create intersection points connected in a graph structure and employing the Dijkstra algorithm. The final path is determined by adding the third dimension as a sum of specified minimum flight altitude and the elevation value of the current position from the map.

A multi-UAV sampling-based Coverage Path Planning (CPP) framework for the inspection of large-scale, complex 3D structures is presented in [28]. The proposed method first generates waypoints and path-primitives by incremental sampling to create a coverage probabilistic roadmap graph with information on topology, coverage, and path length. The multi-agent CPP is then formulated as a min-max set covering the TSP problem and solved by a modified Random Key Genetic Algorithm (RKGA) which optimizes the inspection paths for multiple agents.

3. Three-dimensional ergodic exploration

A multidimensional-dimensional ergodic coverage with the HEDAC method has already been theoretically presented in [12] but all published improvements on HEDAC control are implemented and applied only for two-dimensional problems. Here, we demonstrate trajectory planning for a group of inspection UAVs that operates in a three-dimensional domain $\Omega \in \mathbb{R}^3$ encompassed with the boundary Γ . Physical domain Ω is explored by a swarm of n UAVs and their motion is described with trajectories $\mathbf{y}_i : t \rightarrow \Omega$, where t is time and $i = 1, \dots, n$ are indices of UAVs.

3.1. Space coverage

The three-dimensional coverage can be considered as a continuous action of a UAV along its trajectory. Mathematically this can be defined as a convolution of instantaneous action ϕ

and the trajectory, which results in a field occupying the space around the path of the UAV. For practical reasons, we use a radial basis function, precisely the three-dimensional Gaussian function, as the instantaneous action. The smoothness of the Gaussian function allows better stability and smooth motion because the coverage is accumulated near the trajectory. The use of the Gaussian function in the HEDAC control is utilized and proven in numerical experiments in two-dimensional coverage motion control applications [12, 14, 15]. This instantaneous action can be defined as:

$$\phi_\sigma(r) = \frac{\Phi}{(\sigma\sqrt{2\pi})^3} \exp\left(-\frac{r^2}{2\sigma^2}\right) \quad (1)$$

where Φ is the coverage action intensity, σ is standard deviation or the scope of action function ϕ , and $r_i(t) = \|\mathbf{x} - \mathbf{y}_i(t)\|$ is distance from location in the domain \mathbf{x} to agent's position \mathbf{y} . The intensity can be interpreted via a property of the instantaneous action function: $\int_{\mathbb{R}^3} \phi \, d\mathbf{x} = \Phi$. The coverage field $\rho(\mathbf{x})$ is defined as a convolution integral:

$$\rho(\mathbf{x}, t) = \sum_{i=1}^n \int_0^t \phi_\sigma(r_i(\tau)) \, d\tau. \quad (2)$$

Note that, due to simplicity and practicality, the same action function ϕ_σ is utilized for all agents. Though, it is shown in [14] that HEDAC can be utilized for governing multiple heterogeneous agents in both sensing and motion characteristics.

The objective of space coverage is to produce agents' trajectories that explore the domain according to a given density. Furthermore, we want to enable continuous non-stopping coverage motion whenever the agents' safety constraints are not violated. According to the given target density $\mu_0(\mathbf{x})$, characterizing UAV visiting areas and frequency, one can define exponential law to determine a remaining density μ at time t according to achieved coverage ρ :

$$\mu(\mathbf{x}, t) = \mu_0(\mathbf{x}) \cdot \exp(-\rho(\mathbf{x}, t)). \quad (3)$$

The target density μ_0 is normalized in order to satisfy $\int_{\Omega} \mu_0(\mathbf{x}) \, d\mathbf{x} = 1$. This formulation is analogously used in [14] for defining (undetected) target probability in multi-agent search motion control with uncertain target detection.

The objective of the ergodic exploration is to evenly fill the space with trajectories or to fill it according to a given density. In the proposed formulation (3), minimizing μ does not lead to equalization of target density μ_0 and coverage ρ . However, it is trivial to show that minimizing μ results with $\rho(\mathbf{x}) = \ln(\mu_0(\mathbf{x}))$, i.e. $\ln(\mu_0)$ can be considered as goal density used in [29, 12]. This approach elegantly solves the problems of normalization and logarithm of zero-valued μ_0 which can arise in the conventional ergodic coverage formulation. As stated, in order to realize a spatial coverage, the motion control needs to direct the UAVs in order to accomplish

$$\lim_{t \rightarrow \infty} \int_{\Omega} \mu(\mathbf{x}, t) \, d\mathbf{x} = 0. \quad (4)$$

It is suitable to define the measure for the coverage

$$E(t) = \int_{\Omega} \mu(\mathbf{x}, t) d\mathbf{x} \quad (5)$$

that indicates the share of uncovered space.

3.2. Utilizing a potential field for directing UAVs

In order to achieve the minimization (4) in time, one needs to minimize the μ spatially. HEDAC's main idea is to design a potential field ψ which can facilitate the minimization of μ . The Helmholtz partial differential equation, used for modeling conductive heat transfer accompanied by convective cooling, is employed for obtaining the potential ψ :

$$k \cdot \Delta\psi(\mathbf{x}, t) - \psi(\mathbf{x}, t) + \mu(\mathbf{x}, t) = 0 \quad (6)$$

with Neumann boundary condition applied to the entire boundary:

$$\left. \frac{\partial\psi}{\partial\mathbf{n}} \right|_{\Gamma} = 0 \quad (7)$$

where \mathbf{n} is the boundary outward-pointing normal. The parameter k represents the coefficient of thermal conductivity and regulates global and local details of the resulting potential field. For the purpose of this search model, we will assume this coefficient is dimensionless. Note that more parameters were used in previous HEDAC formulations, but the conduction coefficient is dominantly regulating the behavior of ψ , hence it is reasonable to consider only this parameter of the HEDAC control.

The potential field ψ calculated by (6) is actually a smoothed field μ , which is accomplished due to using the Laplacian operator $\Delta\psi$. This allows us to utilize the gradient of the potential in order to establish the direction to regions of higher potential and implicitly to regions of higher values of density μ . We calculate the desired direction of each UAV motion as a unit gradient of the potential ψ :

$$\mathbf{u}_i(t) = \frac{\nabla\psi(\mathbf{y}_i, t)}{\|\nabla\psi(\mathbf{y}_i, t)\|}, \quad i = 1, \dots, n. \quad (8)$$

Finally, we define a motion model to close the control's feedback loop. The motion, and consequentially the trajectories, are an outcome of 1-st order control, where the position is directly changed by control-appointed direction. This motion model is often called kinematic since it neglects the mass and inertial effects of UAV motion. However, due to advanced low-level multi-rotor control, in practice, modern multi-rotors can make a turn in any direction almost instantaneously. Therefore, it is justified to use such a model for multi-rotor UAV inspection simulations.

Due to Neumann boundary condition (7) following the gradient of the potential $\nabla\psi$ inherently avoids for an agent to approach domain boundaries. However, there is no assurance that the agent will not collide with the boundary due to chosen combination of numerical parameters for solving partial differential equation (6) (such as numerical grid density and time step) and UAV properties (such as agent velocity v and action range σ). Furthermore, a possible collision between two or more UAVs also needs to taken into account when directing multiple UAVs.

3.3. Collision avoidance

Several different approaches for boundary and inter-UAV collision avoidance were successfully utilized in two-dimensional HEDAC applications [12, 15]. When compared to the collision avoidance in two dimensions, the three-dimensional case has more degrees of freedom hence the probability of random collisions between UAVs is greatly reduced but they do occur eventually if no collision avoidance procedure is implemented. We implemented a robust and computationally inexpensive collision avoidance mechanism preventing collisions of agents with other agents and with the domain boundaries.

The possibility of collisions is checked at every time step for i -th agent by measuring the distance $d(i, j) = |\mathbf{e}_{i,j}|$, $i \neq j$ to all other agents indexed with j and the minimal distance of the agent to the domain boundary $d_b(\mathbf{y}_i)$, where $\mathbf{e}_{i,j} = \mathbf{y}_j - \mathbf{y}_i$ and $d(i, i) = \infty$. If the minimum of all measured distances $d(\mathbf{y}_i) = \min(d_b(\mathbf{y}_i), d(i, 1), \dots, d(i, n))$ is below initially prescribed threshold 2ϵ , the collision avoidance must intervene and correct the directional vector of the agent. Safety distance parameter $\epsilon > v_i\Delta t$ must be large enough to enable safe and smooth maneuvers when avoiding collisions and low enough to not interfere significantly with the prime goal. If the agent's distance to obstacles is below the safety distance, it must not be allowed to reduce this distance in the next step.

Let, $I_i = \{j | d(i, j) < 2\epsilon, i \neq j\}$ be a set of indexes of agents for which the i -th agent is in danger of collision and suppose $d_b(\mathbf{y}_i) < 2\epsilon$ i.e. that the i -th agent is also too close to the domain boundary. We would like to find a direction vector \mathbf{w}_i for the i -th agent such that it closes an obtuse angle with vectors $\mathbf{e}_{i,j}$, $j \in I_i$ and vector $\nabla d_b(\mathbf{y}_i)$. Furthermore, to make this vector unique, we can pick the one which is closest to the vector $\mathbf{c} = \sum_{j \in I_i} \mathbf{e}_{i,j} + \nabla d_b(\mathbf{y}_i) + \mathbf{u}_i$.

If we are able to solve this problem, then this direction will lead as away from the boundary and neighboring agents in the next step. This problem can be formulated as an optimization problem:

$$\text{maximize}_{\mathbf{w}_i} \quad \mathbf{c}^T \mathbf{w}_i \quad (9)$$

$$\text{subject to} \quad -\mathbf{A}\mathbf{w}_i \leq \mathbf{0} \quad (10)$$

$$\|\mathbf{w}_i\| = 1, \quad (11)$$

where

$$\mathbf{A} = \begin{bmatrix} \bar{\mathbf{A}} \\ \nabla d_b(\mathbf{y}_i) \\ \mathbf{u}_i \end{bmatrix}$$

and $\bar{\mathbf{A}} = [\mathbf{e}_{i,j}]$, $j \in I_i$.

The solution of this linear objective function with nonlinear constraints can be solved efficiently using a nonlinear solver. Figure 1 shows the feasible space for a matrix A with three rows where each row corresponds to a depicted black vector pointing towards the feasible region. The solution is a unit vector \mathbf{w}_i depicted in red which closes an acute angle with highlighted vectors.

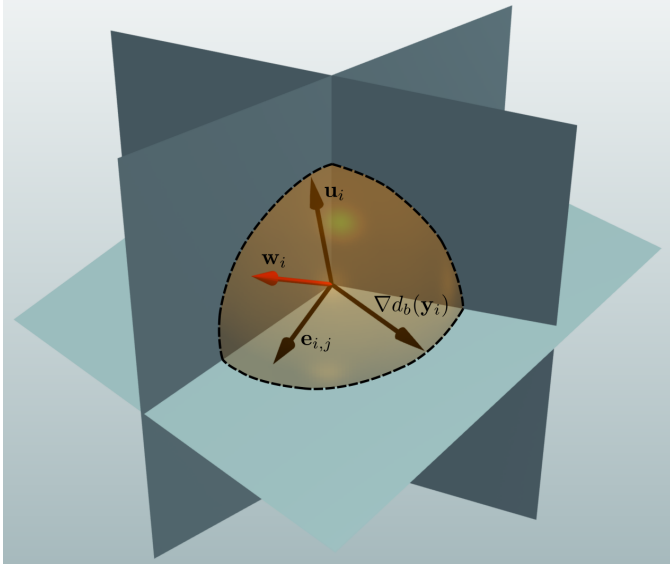


Figure 1: Feasible region for the optimal collision avoidance vector marked with a dashed sphere triangle. The solution \mathbf{w}_i of the optimization problem with nonlinear constraint $\|\mathbf{w}_i\| = 1$ and linear constraints defined by normal vectors \mathbf{u}_i , $\mathbf{e}_{i,j}$ and $\nabla d_b(\mathbf{y}_i)$

It can be shown that the distance from the boundary $d_b \in C^2$, therefore, $\nabla d_b(\mathbf{y}_i)$ always exists and points towards the boundary. We should stress that the matrix \mathbf{A} has at least one row and $\nabla d_b(\mathbf{y}_i)$ will not be included if $d_b(\mathbf{y}_i) \geq \epsilon$. It is possible that the optimization problem does not have a solution because the feasible set is empty. In that case, the matrix \mathbf{A} must have at least 6 rows (conditions) which is highly unlikely in practical situations. In the two-dimensional case, it would take at least 4 rows for this to occur. In the unlikely case that the optimization problem was not solved, the UAV should stand still for this time step and wait for the neighboring agents to clear its path. This maneuver is feasible for a multi-rotor UAV.

An initial approximate solution of the optimization problem is obtained using an approximate linear program which finds a good initial solution candidate in the feasible space. The initial approximate solution is used by a Trust-region optimization implemented in Scipy 1.7.3 [30] which is based on algorithms found in [31]. The solution to this optimization problem is computationally inexpensive and is invoked sparsely therefore it does not add significantly to the overall complexity of the algorithm.

3.4. Defining UAVs' trajectories

The motion of each agent in the fleet of UAVs is defined as:

$$\frac{d\mathbf{y}_i}{dt} = \begin{cases} v_i \cdot \mathbf{w}_i(t) & \text{if } d(\mathbf{y}_i) < \epsilon, \\ v_i \cdot \left(\left(2 - \frac{d(\mathbf{y}_i)}{\epsilon}\right) \mathbf{w}_i(t) + \left(\frac{d(\mathbf{y}_i)}{\epsilon} - 1\right) \mathbf{u}_i(t) \right) & \text{if } \epsilon \leq d(\mathbf{y}_i) < 2\epsilon, \\ v_i \cdot \mathbf{u}_i(t) & \text{otherwise,} \end{cases} \quad (12)$$

where v is a constant velocity of all quad-rotors, and \mathbf{w}_i is the direction obtained as a solution to collision avoidance nonlinear optimization problem.

The collision avoidance can cause jitters in the trajectories because it is not applied smoothly. To fix this problem and smooth out trajectories, the correction of the direction vector is applied gradually when the minimal distance satisfies $d(\mathbf{y}_i) \in [\epsilon, 2\epsilon)$. In the unlikely case that the agent gets too close to an obstacle, the collision-avoidance direction vector is applied to move the agent toward a collision-safe part of the domain.

3.5. Numerical implementation using finite element method

The numerical solution of equation (6) together with boundary condition (7) can be complicated to solve, especially if the geometry of the boundary is complex. In practical applications of this model, we use a connected 3D domain with holes that can have complex geometry. Furthermore, for practical applications, we need a relatively large number of numerical grid points. FEM provides a simple implementation of boundary conditions, a fast solver, and a straightforward interpolation of results on any given grid.

The weak formulation of the presented problem is obtained by multiplying the equation (6) by a smooth test function $v \in H^1(\Omega)$, $\Omega \subset \mathbb{R}^3$ and integrating over the domain. Using the integration by parts, the following equation is obtained:

$$-k \int_{\Omega} \nabla \psi(\mathbf{x}, t) \nabla v(\mathbf{x}) \, d\Omega - \int_{\Omega} \psi(\mathbf{x}, t) v(\mathbf{x}) \, d\Omega + \int_{\Omega} \mu(\mathbf{x}, t) v(\mathbf{x}) \, d\Omega + \sum_{j=0}^{n_0} \oint_{\Gamma_j} (\nabla \psi(\mathbf{x}, t) \cdot \boldsymbol{\eta}) v(\mathbf{x}) \, d\Gamma = 0.$$

The final form of weak formulation is obtained after we apply the Neumann boundary for all parts of the boundary $\Gamma_j \subset \Gamma$:

$$\int_{\Omega} k \nabla \psi(\mathbf{x}, t) \nabla v(\mathbf{x}) + \psi(\mathbf{x}, t) v(\mathbf{x}) - \mu(\mathbf{x}, t) v(\mathbf{x}) \, d\Omega = 0. \quad (13)$$

We will use quadratic polynomials for the space of test functions and our representation of the solution. Let $M = \{T_1, \dots, T_N\}$ be a partition of Ω into N uniform non-overlapping triangles. The triangles with the geometry described by the classical 3-node interpolation functions. The scalar field of the unknown variable and test functions over each n -node element T_i is approximated by

$$\psi_h = \sum_{j=1}^n N_j u_j$$

where N_j stands for the Lagrangian polynomial interpolation functions.

Because the domain and the triangulation do not change during the entire calculation, the linear system coefficient matrix is sparse and constant hence the solutions are obtained very efficiently. Interpolation of different scalar fields and the calculation of the gradient $\nabla \psi$ can be directly obtained using a finite element representation [32]. All results were obtained using the latest version of the finite element software NGSolve.

3.6. 3D coverage examples

The proposed algorithm can be used to cover a three-dimensional space with a given density of trajectories. To demonstrate this application we will use a simple unit cube domain and 100 agents initially distributed randomly in the center of the cube. The density of the trajectories must uniformly fill the lower part of the cube where $0.05 < x, y < 0.95$ and $0.05 < z < 0.45$. This test was created to demonstrate that this algorithm can avoid collisions inside a crowded domain without sacrificing the goal of space exploration. The safety distance is set to 0.025 m and the velocity is constant 0.1 m/s. Total simulation time is 2000s with time step $\Delta t = 1$ s. and conduction parameter $k = 0.1$.

Figure 2 shows the final result after 50 s and 1000 s. One can observe that the trajectories form a space-filling curve and the agents keep inside the goal area except for a short initial part of the trajectory. This domain is crowded with agents but the trajectories are very smooth and no deadlocks or jitters in the produced trajectories were observed.

Figure 3 clearly shows that the given domain is explored efficiently and the collision avoidance is working properly in this crowded domain. The agents safely navigate the domain and avoid other agents in the process. We must emphasize that the agents, in this case, are more in danger of colliding with each other than the domain boundary. This is a simple artificial test example, but the results demonstrate the algorithm is ready to be tested in a more realistic setting with complex geometries.

4. UAV visual inspection applications

The main task in the visual inspection is to capture all surfaces of the structure using a camera mounted on the UAV. This requires control of the direction of the camera depending on the position of the drone relative to the observed structure. We propose a rather simple idea that considers the control of camera orientation, along already known UAV trajectory, by directing the camera view to the nearest point of the observed structure.

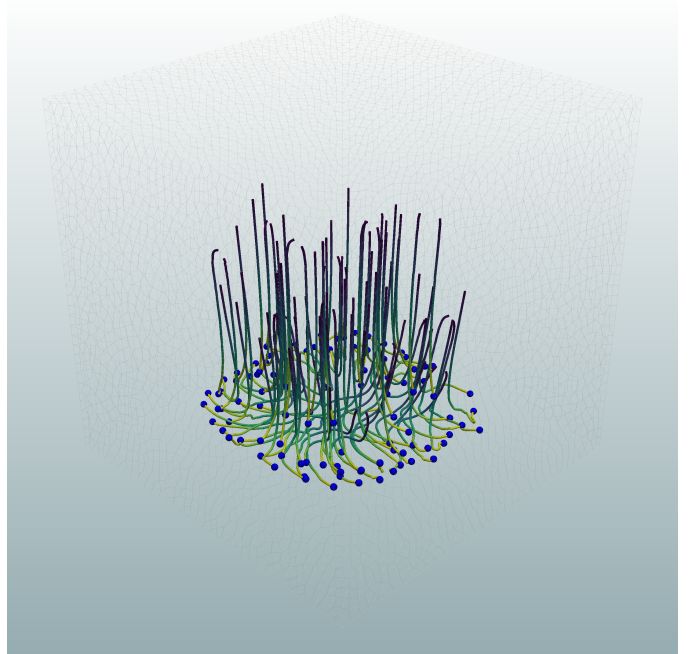
In order to demonstrate the applicability of the proposed algorithm to infrastructure inspection, inspection simulations for three different test cases with varying complexity were conducted.

4.1. Area of interest and camera control for 3D structure inspection

The proposed camera direction control can provide relatively good results if trajectories obtained by HEDAC suitably explore the region around the structure. Since the inspection is acting on faces and surfaces of the investigated structure, the scope of required trajectories can not be correctly transferred to the three-dimensional domain Ω , but the proposed approximation provides satisfactory results.

Similar to the d_b field, we design a field $d_s(\mathbf{x})$ to define the nearest distance from any point of the domain \mathbf{x} to the surface of a structure. Now, we can define a suitable region of interest

(A)



(B)

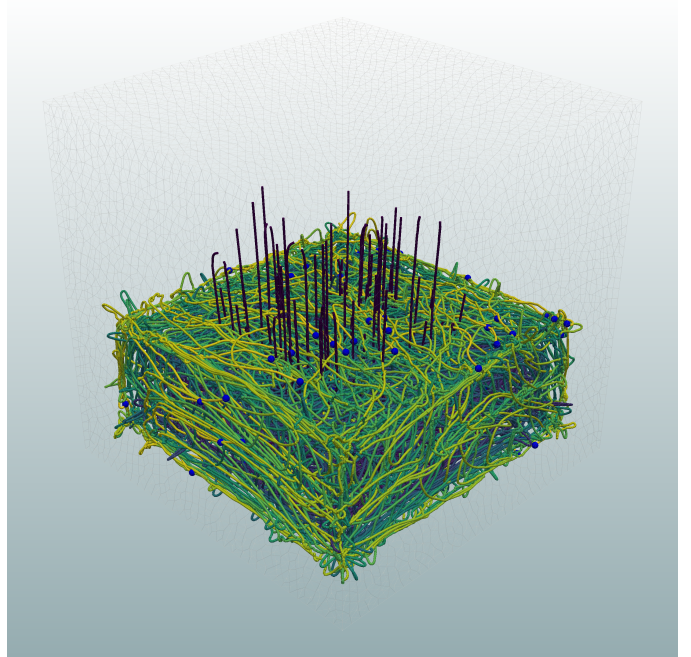


Figure 2: Trajectories of 100 agents after 50 (A) and 1000 seconds (B) produced with HEDAC method for uniform coverage of lower half of the unit cube.

around the observed structure using a three-dimensional Gaussian function:

$$\mu_0(\mathbf{x}) = \exp\left(-\frac{(d_s(\mathbf{x}) - \bar{d})^2}{2 \cdot \bar{d}^2}\right) \quad (14)$$

where \bar{d} is the goal inspection distance at which Gaussian function is centered and \bar{d} is the standard deviation i.e. the broadness of the field μ_0 encompassing the structure. Using (14) al-

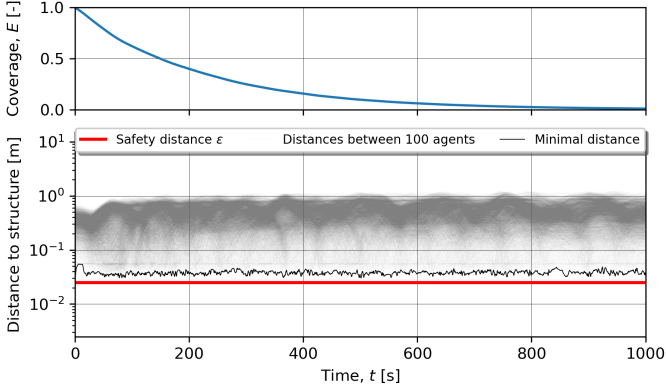


Figure 3: The convergence of the coverage measure E and computed UAV distances during the inspection of the simple unit cube with 100 agents.

allows us to construct a continuous non-negative field around the entire structure, with a peak exactly at the distance \bar{d} from the surfaces to be inspected and gradually weakening both towards and away from the structure. Note that scaling constants are omitted from Gaussian function in (14) since μ_0 is subject to normalization that produces compliant scaling constants.

Finally, we can easily find a camera orientation \mathbf{z}_i for each UAV, as the direction towards the nearest point on the structure, by employing the gradient of the field d_s :

$$\mathbf{z}_i(\mathbf{y}_i) = \frac{\nabla d_s(\mathbf{y}_i)}{\|\nabla d_s(\mathbf{y}_i)\|}.$$

Note that only camera orientation is subjected to the proposed control and provided by the unit vector \mathbf{z} . This approach does not evaluate the field of view, camera focus, zoom, or other details regarding photographic equipment for visual inspection.

4.2. Portal test case

The portal test case is a scenario for visual inspection of a relatively simple synthetic three-dimensional structure. It can be described as a flattened box ($50 \times 70 \times 10$ m) with a rectangular hole in it (30×50 m), and it is designed to provide a simple shape while requiring relatively complex maneuvers to achieve structure inspection. The target density field μ_0 (Figure 4) is defined using goal inspection distance $\bar{d} = 5$ m and broadness $\bar{d} = 2$ m. Other info and parameters used for the portal case simulation are presented in Table 1.

The proposed algorithm for path planning of visual inspection of the portal structure is conducted for 3 UAVs in the duration of 1 500 s achieving convergence of the three-dimensional coverage, for the given μ_0 , as shown in Figure 5(A).

Plotted distance lines indicate that generated UAVs paths around the structure are, on average, at distance $\bar{d} = 5$ m from the structure. However, it can be observed that distances slightly increase, on average, during the inspection. The target density μ_0 is computed to form a region at the offset from the structure's surface which is mostly convex. The resulting potential field ψ is positioned slightly closer to the structure than μ_0 on the convex part of the structure's surface, due to the smoothing effect of the Laplacian operator in the Helmholtz equation.

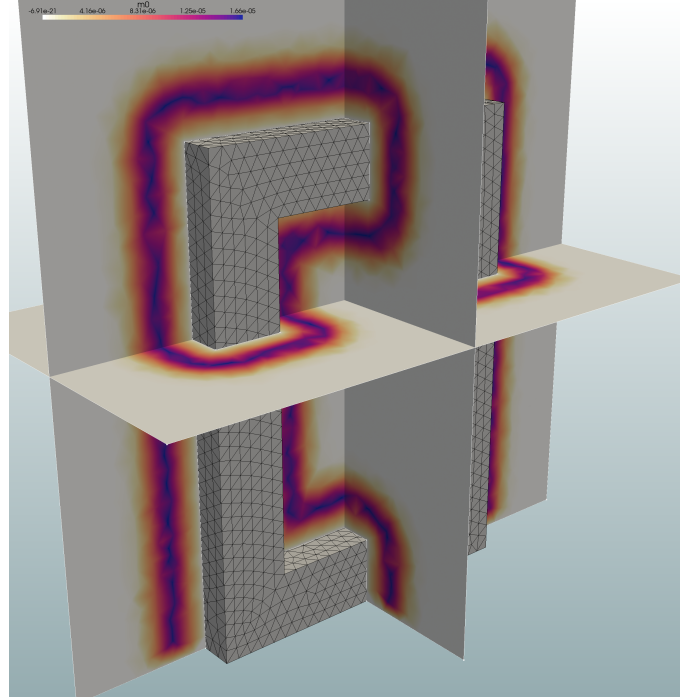


Figure 4: The target density field μ_0 , of thickness $\bar{d} = 2$ m, encompasses the portal structure at the distance $\bar{d} = 5$ m.

Parameter	Value	Unit
Structure length	10	m
Structure width	50	m
Structure height	70	m
Domain length	50	m
Domain width	90	m
Domain height	90	m
Number of domain mesh nodes	34 161	
Number of domain mesh elements	167 495	
Number of structure mesh surface nodes	2 315	
Number of structure mesh surface faces	4 630	
Inspection distance \bar{d}	5	m
Inspection distance broadness \bar{d}	2	m
Number of UAVs	3	
UAV velocity v	0.5	m/s
Safety distance ϵ	1	m
Coverage action intensity Φ	200	
Coverage action range σ	5	m
HEDAC conduction coefficient k	12	
Inspection duration	1 500	s
Path planning time step Δt	1	s

Table 1: Domain, structure and numerical mesh info, inspection task parameters, UAV parameters, and HEDAC parameters used in the portal test case.

Consequently, the outcome is UAVs' paths that are closer to the structure than appointed \bar{d} . After first rough passes around the structure, which are relatively close to it, the remaining density μ is now more accumulated at a distance greater than \bar{d} from the inspected surfaces. Thus, in the second part of the inspection operation, UAVs paths are generated at a greater distance from the structure. The distances of produced paths are safely kept above the minimal safety distance ϵ during the entire operation.

Due to the large proportions of structure and domain, distances between UAVs are practically negligible in the context of the minimum allowable spacing constraint.

The produced trajectories \mathbf{y}_i and accompanying camera orientations \mathbf{z}_i for all three UAVs are displayed in Figure 5(B). Note that the unit vector of camera orientation is scaled to the length equal to the inspection distance \bar{d} . The produced trajectories are smooth and suitably distanced from the structure complying given target density field μ_0 presented in Figure 4.

Based on the camera orientation visualization shown in Figure 5(B), all surfaces of the inspected structure are observed relatively uniformly, which brings to the conclusion that planned paths and camera orientations are suitable for inspection application.

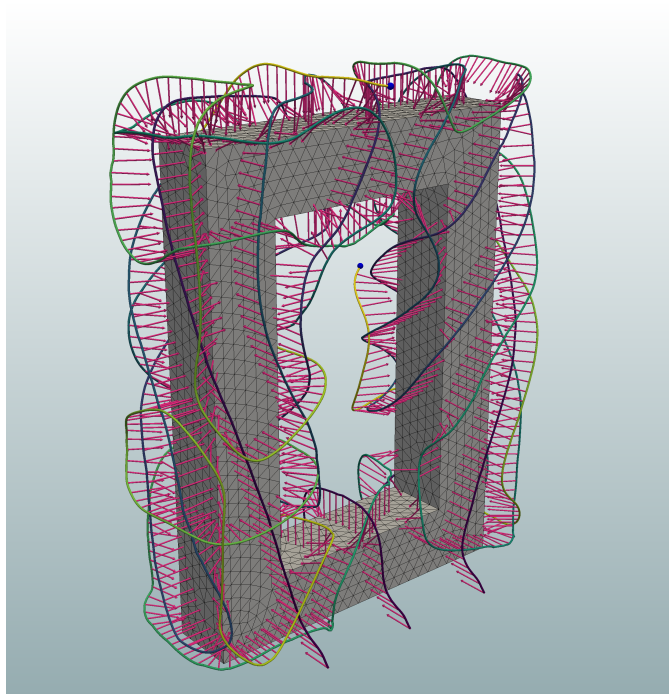
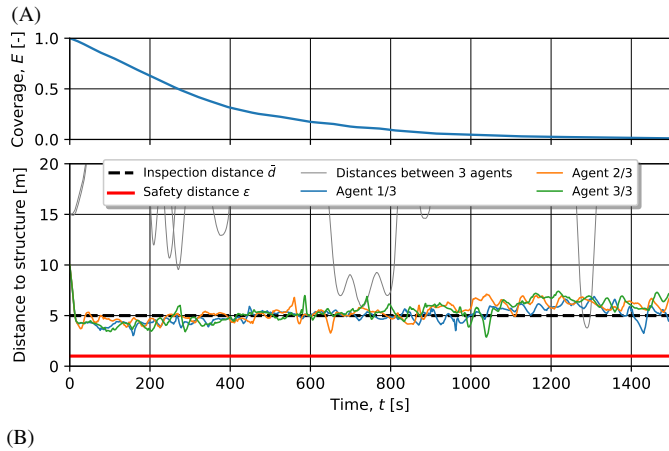


Figure 5: (A) The convergence of the coverage measure E and computed UAV distances during the inspection. (B) shows trajectories of three UAVs performing inspection of the portal structure after 1 500 s. Camera orientations along trajectories are displayed as magenta arrows of length equal to inspection distance \bar{d} .

4.3. Wind turbine test case

Wind turbine inspection with UAV technology has become the norm in the past several years as it provides a lot of benefits over manual or ground-based inspection. The main advantages include human safety and high-quality inspection data with a noticeable reduction in data acquisition time. Furthermore, the given benefits of the UAV-based inspection approach enable a reduction in maintenance costs of wind turbine farms [33]. Due to the given rationale, a number of previous studies have included a wind turbine test case to assess the quality and efficiency of their respective visual inspection algorithms [34, 26, 35, 24], and hence in this paper, a wind turbine 3D visual inspection case is also presented.

For the wind turbine test case, a path planning for the inspection using two UAVs is prepared according to the parameters shown in Table 2. The structure of the wind turbine consists of a 120 m high vertical column, a hub, and three attached blades, each 80 m long. Blades are rotated at a 60° angle, forming an "upside-down Y" shape, which is a typical orientation for the inspection operations. Based on the shape of the wind turbine structure, the inspection distance \bar{d} and broadness \tilde{d} , the target density field μ_0 used for governing the flying regions for the inspection is computed (Figure 6). Note that the numerical domain used in this test case is significantly larger than the space needed for inspection flight in order to allow for the UAV to directly pass from the tip of one blade to the tip of another blade (or to the root of the column), though this possibility is not utilized in performed path planning computations.

Parameter	Value	Unit
Structure length	25.6	m
Structure width	122.8	m
Structure height	203.1	m
Domain length	65.9	m
Domain width	162.9	m
Domain height	223.1	m
Number of domain mesh nodes	124 979	
Number of domain mesh elements	711 003	
Number of structure mesh surface nodes	11 052	
Number of structure mesh surface faces	22 100	
Inspection distance \bar{d}	6	m
Inspection distance broadness \tilde{d}	1	m
Number of UAVs	2	
UAV velocity v	1.2	m/s
Safety distance ϵ	1	m
Coverage action intensity Φ	400	
Coverage action range σ	3	m
HEDAC conduction coefficient k	5	
Inspection duration	1 200	s
Trajectory planning time step Δt	0.5	s

Table 2: Parameters for the wind turbine inspection scenario containing domain, structure and numerical mesh info, inspection task parameters, UAV parameters, and HEDAC parameters.

The wind turbine inspection typically takes about 40 minutes during which about 1000 photographs of the turbine surface are recorded. In this inspection scenario, a pair of UAVs is used in order to speed up the inspection operation (the duration is

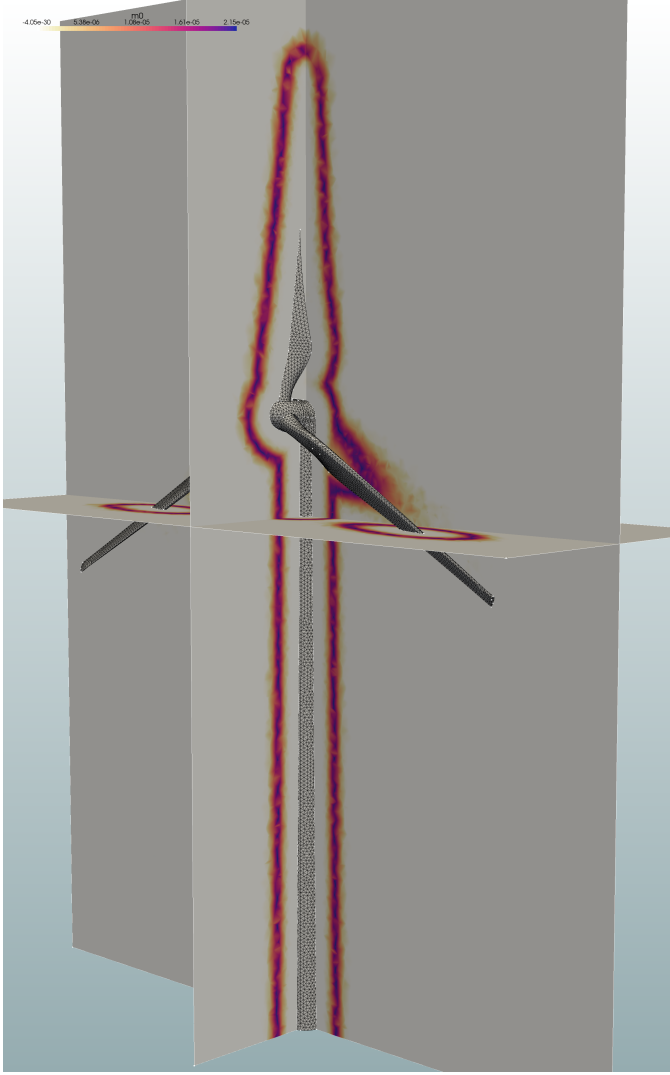


Figure 6: The μ_0 field for wind turbine test case defines the region aimed to be occupied by UAVs' trajectories along which all turbine structure faces can be inspected.

20 minutes) and to demonstrate the coordination between two UAVs on a relatively slender structure such as a wind turbine.

A slightly stepped convergence of the coverage E can be observed in Figure 7(A) due to the UAVs' inspection focus switching between the wind turbine's column, hub, and blade. The Y-shaped configuration of wind turbine structure components is causing multi-pass inspections of individual components of the turbine, where each subsequent pass produces flatter change in E and finally, it results in stepped coverage performance. Analogous to the first example, the distances of the paths from the structure are on average equal to $\bar{d} = 6$ m and they have an increasing trend during the inspection. Since the path planning is performed only for two UAVs and the domain is considerably large, the spacing between UAVs is easily kept at the safe distance ϵ .

Realized trajectories and camera orientations for wind turbine inspection are shown in Figure 7(B). It is interesting to observe a synchronized spiral motion caused by the interaction

between UAVs' coverage actions. All components of the turbine structure are observed from practically all directions and UAVs effectively collaborate in the inspection. The presented results imply that the proposed HEDAC trajectory planning algorithm is suitable for carrying out a multi-UAV inspection on real-world structures such as wind turbines.

4.4. Bridge test case

Bridge inspection using UAVs is commonly conducted to visually detect damage as it lowers the inspection costs and increases safety. Usually, UAVs are flown manually to visually inspect the structure using sensors and cameras. There has been a rising interest in research of UAV autonomous bridge inspection where previous studies have attempted to provide path planning and trajectory planning algorithms [19]. The most noticeable one is receding horizon next-best-view planner [22] which is described in Section 2. The authors employ the algorithm both for the exploration of a domain containing an unknown structure and for the visual inspection of a known structural model. For the inspection test case, the environment is represented as a volumetric occupancy grid map where segments are marked as inspected or uninspected based on the sensors readings within 10 m, and paths are planned accordingly. To achieve greater coverage and improve computational performance, the planner produces paths by taking into account sensor readings at a distance of 2 m. Colliding box around the agent assures a safe distance between the agent and the structure. Visual inspection of a bridge structure using a single UAV lasted for $t_{tot} = 105.0$ min and achieved coverage of 99.1%. Within this section, we reconstruct the same bridge test case, adapt it for HEDAC, and calculate the inspection paths with proper camera orientations. All parameters we used for the bridge test case and their analogies from [22] are provided in Table 3.

The structure consists of around 50 m long and 13 m wide bridge deck as well as two 9 m high arches, increasing the inspection complexity when compared to the portal or wind turbine cases. The inspection domain is represented with the distance field inside the domain size volume. The distance field contains distances from the structure; therefore, leading agents near the structure to inspect. Based on the distance field d_s , we calculate the target density μ_0 that covers the space around all structural components of the bridge at the distance \bar{d} with broadness \bar{d} as shown in Figure 8. The implemented collision avoidance algorithm prevents agent-to-agent collision as well as agent-to-boundary and agent-to-structure collisions. Besides the single UAV bridge inspection simulation, we also run simulations of simultaneous visual inspection using five UAVs. Produced trajectories for both cases are visualized in Figure 10, showing appropriate camera orientations along the trajectories.

The convergence of the coverage measure E and distances from agents to the structure for both simulations are shown in Figure 9. The inspection distance is difficult to maintain during the operation due to the complex structure and flight domain. However, the agents are restricted with the safety distance assuring the collision avoidance. In a few brief moments, the safety distance is violated while inspecting the bridge with

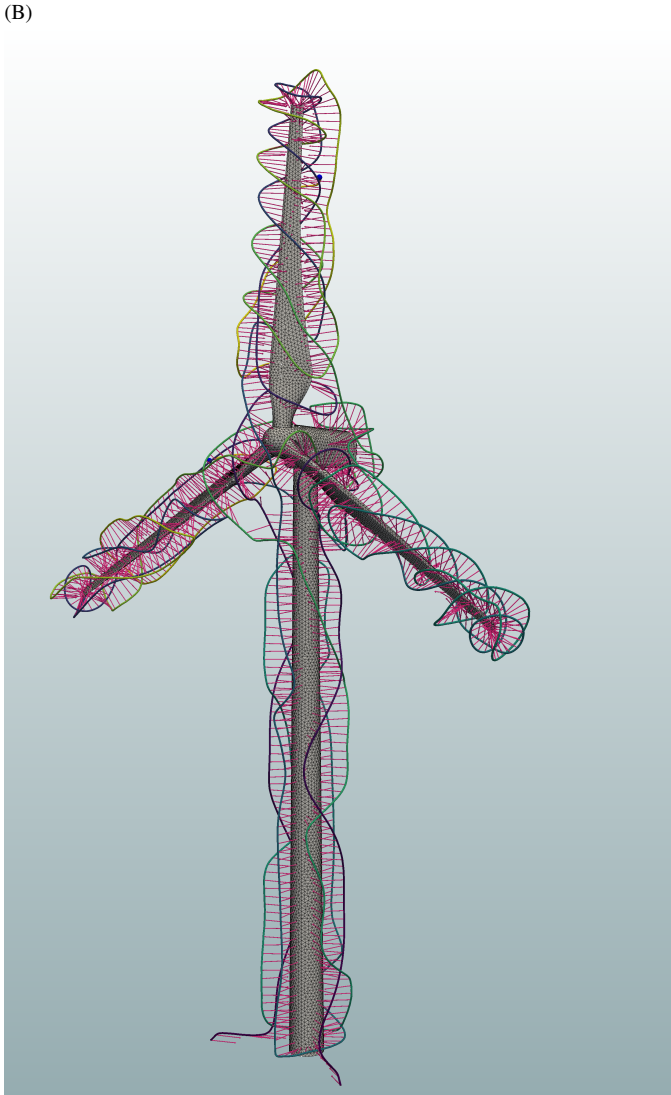
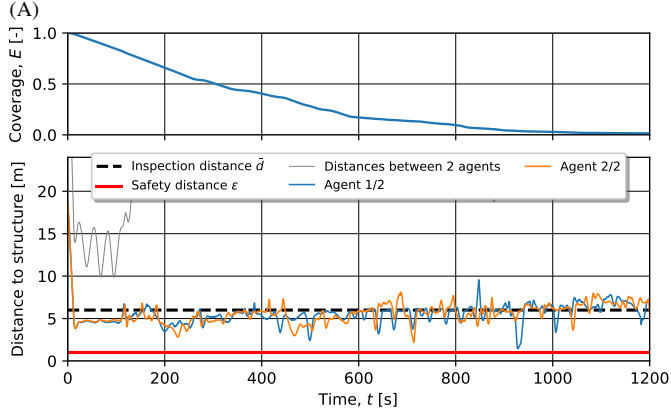


Figure 7: A stepped convergence of the coverage measure E displayed in the plot (A) is caused by inspection motion along relatively isolated parts (column, hub, and blades) of the wind turbine structure. The plot of distances shows that, on average, the inspection distance is ensured and the minimal spacing constraint is complied. Trajectories of two UAVs generated by the HEDAC method for the inspection of the portal structure in a total duration of 1 500 s are shown in (B). Camera orientations along trajectories are displayed as magenta arrows of length equal to inspection distance $\bar{d} = 6$ m.

Parameter	Value	Unit
Structure length	47.5	m
Structure width	12.85	m
Structure height	9.0	m
Domain length	58.3, 50*	m
Domain width	22.85, 25*	m
Domain height	19.9, 14*	m
Number of domain mesh nodes	93 539	
Number of domain mesh elements	503 852	
- Based on volumetric map resolution [22]	1 120 000*	
- Based on inspection mesh resolution [22]	140 000*	
Number of structure mesh surface nodes	23 971	
Number of structure mesh surface faces	48 118	
Inspection distance \bar{d}	1.5	m
- $d_{planner_max}$ [22]	2*	m
Inspection distance broadness \tilde{d}	0.3	m
Number of UAVs	1 ^a , 5 ^b	
UAV velocity v	0.5, 0.5*	m/s
Safety distance ϵ	0.5	m
- Colliding box [22]	0.5 × 0.5 × 0.3*	m
Coverage action intensity Φ	1 ^a , 0.4 ^b	
Coverage action range σ	1	m
- d_{sensor_max} [22]	10*	m
HEDAC conduction coefficient k	20	
Inspection duration	3 000 ^a , 1 000 ^b	s
Path planning time step Δt	0.5	s

Table 3: Geometry and numerical mesh info and parameters used for two variants of the bridge test case (values specific for inspection using a single and five UAVs are marked with ^a and ^b superscript, respectively) and corresponding or analogous parameters used in [22] (marked with *).

five agents due to the crowded flight domain, complex geometry, and a large time step preventing the collision avoidance from the earlier activation. It can be avoided by reducing the time step or employing lesser agents for the inspection. As expected, five UAVs inspecting the bridge structure achieve coverage faster, in around 10 minutes, when compared with using a single UAV which takes around 50 minutes for the inspection. Although it is not directly comparable to the receding horizon planner [22] due to the different coverage measures, it is worth noticing that it takes less time for the inspection of the bridge structure with the HEDAC approach.

5. Conclusion

Due to the fast development of UAV technology and potential cost benefits it could bring, autonomous tasks are prominent topics for contribution to the industries such as civil infrastructure inspection or search and rescue operations. To enable autonomous flight, safe paths need to be determined and provided to the UAVs assuring collision avoidance within the environment. In this paper, we have presented a new method for multiple UAV trajectory planning within a known three-dimensional environment as well as its application for autonomous exploration and visual inspection. The method is an extension of the HEDAC algorithm, previously developed and tested for the exploration of two-dimensional domains. The presented algorithm calculates trajectories that cover three-dimensional space

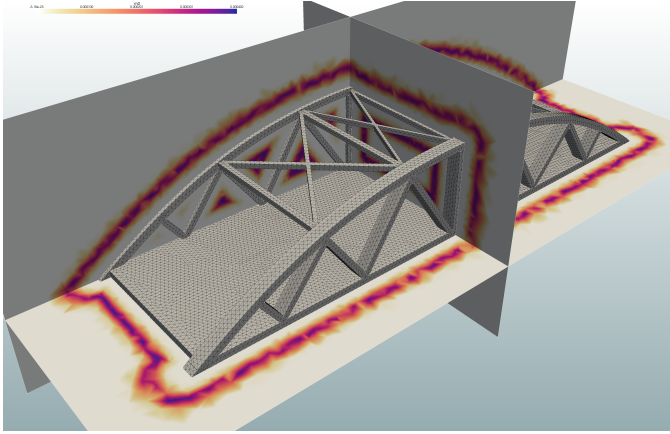


Figure 8: Spatial regions for bridge inspection path planning are defined using detailed target density field μ_0 . The field is constructed around the structure at the distance $\bar{d} = 1.5$ m and with inspection broadness $\bar{d} = 0.3$ m.

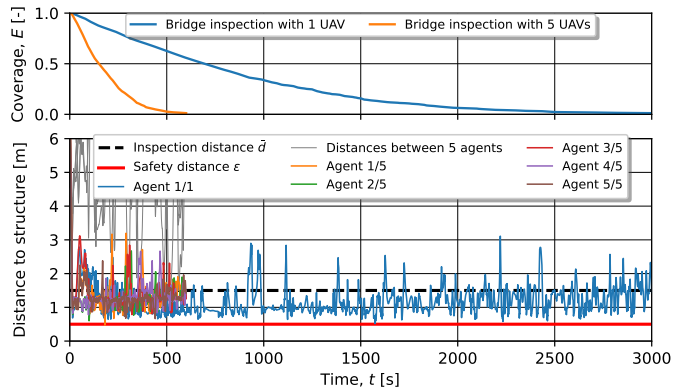


Figure 9: Top subplot show the convergence of coverage E for two scenarios of the bridge inspection: using a single UAV and using five UAVs. The utilization of five UAVs for bridge inspection expectedly converges faster and allows almost ideal scalability, referring to number of UAVs, of the proposed method. Calculated distances for both simulations are shown in bottom subplot. It is clearly visible that inspection distance $\bar{d} = 1.5$ m is hard to maintain during the operation due to highly detailed and complex structure and flight domain. Although not so evident as in previous cases, the increasing trend of UAV-structure distance is also present during the bridge inspection operation.

according to the given target density. The UAV motion is represented using a simple, first-order kinematic model allowing the calculation of trajectories feasible for a UAV. Collision avoidance is formulated as a non-linear optimization problem, successfully preventing collisions between UAVs as well as UAVs with domain boundaries by gradually redirecting a UAV when the distance threshold is reached. We have validated the implementation of collision avoidance in a crowded, unit cube domain with 100 UAVs uniformly covering the lower half of the cube.

We have further adapted the algorithm for the visual inspection of three-dimensional structures using UAVs. In mathematical terms, the task is to explore two-dimensional manifolds embedded in a bounded three-dimensional volume using sensors mounted on a UAV, e.g., a camera. We have achieved this by constructing a three-dimensional field of interest (target density) as an offset from the structure's surface to be inspected.

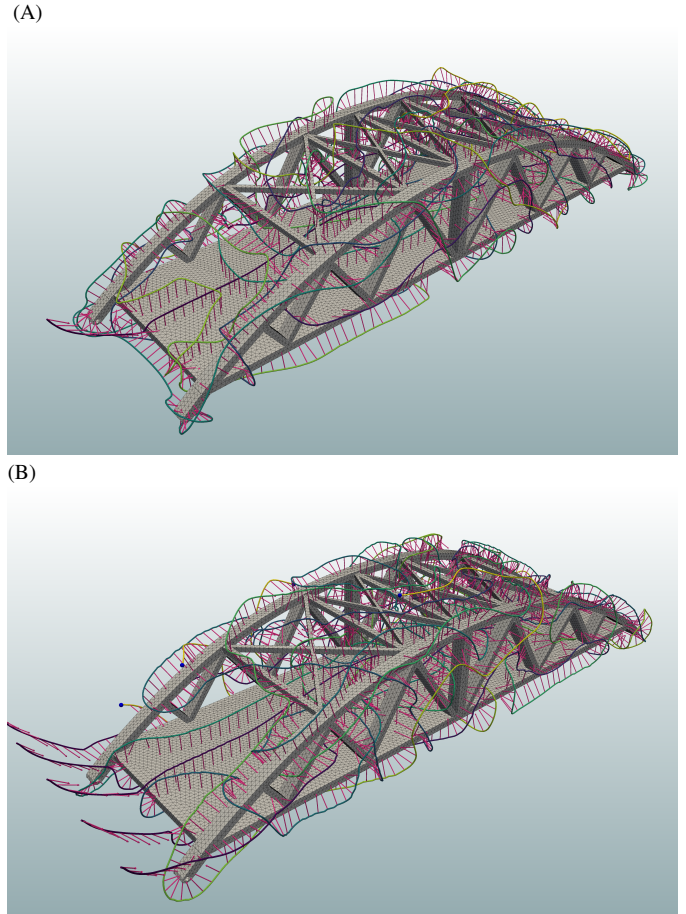


Figure 10: Obtained paths for single UAV (subplot A) and five UAVs (subplot B) bridge inspection planning. The paths successfully explore the domain and avoids frame trusses of the bridge structure. The directions of cameras are suitably adjusted and directed towards almost all surfaces of the bridge structure.

We have proposed a simple idea for handling the camera orientation: it relies on the gradient of the distance field d_s , containing distances to the nearest surface of the inspected structure. This solution produces camera orientations always pointing to the nearest point on the inspected structure.

The proposed method has been tested on three inspection applications. The first test involves a synthetic portal scenario with 3 UAVs inspecting the structure. For a given target density field, the coverage convergence is achieved in 1500 seconds producing smooth trajectories, safely distanced from the structure. All surfaces of the structure are covered relatively uniformly, leading to the conclusion that planned trajectories and camera orientations are suitable for infrastructure inspection with appropriate camera equipment. The second scenario of a wind turbine inspection provides a realistic test case demonstrating the coordination of 2 UAVs inspecting a relatively slender structure. Compared with the smooth coverage convergence in the portal scenario, a slightly stepped coverage convergence is achieved in 20 minutes as a result of inspection focus switching between differently shaped surfaces of a wind turbine (column, hub, and blades). As all components of the wind turbine are observed, we can implicatively conclude that the algorithm

is suitable for conducting an autonomous UAV inspection of real-world structures. The third scenario of a bridge inspection has been conducted with 1 and 5 UAVs inspecting the structure.

Trajectories obtained with the proposed planner, though seemingly chaotic, are uniformly exploring the region around the 3D structure and allow the inspection of all surfaces of the structure. The convergence of the coverage measure is achieved for each scenario, with convergence time depending on the complexity of the inspection structure and the number of UAVs inspecting the structure. The method is proven to be robust and stable, though it is not computationally efficient enough for real-time motion control applications. Some ideas for further research related to this topic, such as better domain mesh generation, solving potential using General-Purpose computing on Graphics Processing Units (GPGPU), or domain partitioning, could potentially raise computational efficiency enough for motion control implementation of the proposed method that is able to compute in real-time.

Acknowledgements

This research is primarily supported by the Croatian Science Foundation under the project UIP-2020-02-5090. B.C. contribution is supported by Croatian Science Foundation under the project IP-2019-04-1239, L. M.'s contribution is supported by the European Union's Horizon 2020 Research and Innovation Programme under Grant Agreement No 861111, Drones4Safety.

Data availability

All parameters for reproducing the study are presented in the manuscript. The data needed to reproduce the presented method and cases are available on the Open Science Framework repository: <https://osf.io/bdrvn/>.

References

- [1] M. Moshref-Javadi, M. Winkenbach, Applications and research avenues for drone-based models in logistics: A classification and review, *Expert Systems with Applications* 177 (2021) 114854.
- [2] S. Bičići, M. Zeybek, An approach for the automated extraction of road surface distress from a uav-derived point cloud, *Automation in Construction* 122 (2021) 103475.
- [3] S. Zhao, F. Kang, J. Li, C. Ma, Structural health monitoring and inspection of dams based on uav photogrammetry with image 3d reconstruction, *Automation in Construction* 130 (2021) 103832.
- [4] D. Kim, M. Liu, S. Lee, V. R. Kamat, Remote proximity monitoring between mobile construction resources using camera-mounted uavs, *Automation in Construction* 99 (2019) 168–182.
- [5] I. Martinez-Alpiste, G. Golcarenenrenji, Q. Wang, J. M. Alcaraz-Calero, Search and rescue operation using uavs: A case study, *Expert Systems with Applications* 178 (2021) 114937.
- [6] S. W. Cho, H. J. Park, H. Lee, D. H. Shim, S.-Y. Kim, Coverage path planning for multiple unmanned aerial vehicles in maritime search and rescue operations, *Computers & Industrial Engineering* 161 (2021) 107612.
- [7] J. F. Falorca, J. P. Miraldes, J. C. G. Lanzinha, New trends in visual inspection of buildings and structures: Study for the use of drones, *Open Engineering* 11 (1) (2021) 734–743.
- [8] A. Gasparetto, P. Boscaroli, A. Lanzutti, R. Vidoni, Path planning and trajectory planning algorithms: A general overview, *Motion and operation planning of robotic systems* (2015) 3–27.
- [9] E. Galceran, M. Carreras, A survey on coverage path planning for robotics, *Robotics and Autonomous systems* 61 (12) (2013) 1258–1276.
- [10] R. Almadhoun, T. Taha, L. Seneviratne, Y. Zweiri, A survey on multi-robot coverage path planning for model reconstruction and mapping, *SN Applied Sciences* 1 (8) (2019) 1–24.
- [11] M. Torres, D. A. Pelta, J. L. Verdegay, J. C. Torres, Coverage path planning with unmanned aerial vehicles for 3d terrain reconstruction, *Expert Systems with Applications* 55 (2016) 441–451.
- [12] S. Ivić, B. Crnković, I. Mezić, Ergodicity-based cooperative multiagent area coverage via a potential field, *IEEE transactions on cybernetics* 47 (8) (2016) 1983–1993.
- [13] S. Ivić, A. Andrejčuk, S. Družeta, Autonomous control for multi-agent non-uniform spraying, *Applied Soft Computing* 80 (2019) 742–760.
- [14] S. Ivić, Motion control for autonomous heterogeneous multiagent area search in uncertain conditions, *IEEE Transactions on Cybernetics* (2020).
- [15] S. Ivić, A. Sikirica, B. Crnković, Constrained multi-agent ergodic area surveying control based on finite element approximation of the potential field, *arXiv preprint arXiv:2109.10756* (2021).
- [16] Z. Shang, J. Bradley, Z. Shen, A co-optimal coverage path planning method for aerial scanning of complex structures, *Expert Systems with Applications* 158 (2020) 113535.
- [17] M. D. Phung, C. H. Quach, T. H. Dinh, Q. Ha, Enhanced discrete particle swarm optimization path planning for uav vision-based surface inspection, *Automation in Construction* 81 (2017) 25–33.
- [18] C. Cao, J. Zhang, M. Travers, H. Choset, Hierarchical coverage path planning in complex 3d environments, in: *2020 IEEE International Conference on Robotics and Automation (ICRA)*, IEEE, 2020, pp. 3206–3212.
- [19] L. Shi, G. Mehrooz, R. H. Jacobsen, Inspection path planning for aerial vehicles via sampling-based sequential optimization, in: *2021 International Conference on Unmanned Aircraft Systems (ICUAS)*, IEEE, 2021, pp. 679–687.
- [20] dmishin/tsp solver, [Suboptimal travelling salesman problem \(tsp\) solver](https://github.com/dmishin/tsp-solver), accessed: 2022-02-24. URL <https://github.com/dmishin/tsp-solver>
- [21] S. Jung, S. Song, P. Youn, H. Myung, Multi-layer coverage path planner for autonomous structural inspection of high-rise structures, in: *2018 IEEE/RSJ International Conference on Intelligent Robots and Systems (IROS)*, IEEE, 2018, pp. 1–9.
- [22] A. Bircher, M. Kamel, K. Alexis, H. Oleynikova, R. Siegwart, Receding horizon path planning for 3d exploration and surface inspection, *Autonomous Robots* 42 (2) (2018) 291–306.
- [23] A. Bircher, K. Alexis, M. Burri, P. Oettershagen, S. Omari, T. Mantel, R. Siegwart, Structural inspection path planning via iterative viewpoint resampling with application to aerial robotics, in: *2015 IEEE International Conference on Robotics and Automation (ICRA)*, IEEE, 2015, pp. 6423–6430.
- [24] A. Bircher, M. Kamel, K. Alexis, M. Burri, P. Oettershagen, S. Omari, T. Mantel, R. Siegwart, Three-dimensional coverage path planning via viewpoint resampling and tour optimization for aerial robots, *Autonomous Robots* 40 (6) (2016) 1059–1078.
- [25] H. Baik, J. Valenzuela, Unmanned aircraft system path planning for visually inspecting electric transmission towers, *Journal of Intelligent & Robotic Systems* 95 (3) (2019) 1097–1111.
- [26] S. S. Mansouri, C. Kanellakis, E. Fresk, D. Kominiak, G. Nikolakopoulos, Cooperative coverage path planning for visual inspection, *Control Engineering Practice* 74 (2018) 118–131.
- [27] H. I. Perez-Imaz, P. A. Rezeck, D. G. Macharet, M. F. Campos, Multi-robot 3d coverage path planning for first responders teams, in: *2016 IEEE International Conference on Automation Science and Engineering (CASE)*, IEEE, 2016, pp. 1374–1379.
- [28] W. Jing, D. Deng, Y. Wu, K. Shimada, Multi-uav coverage path planning for the inspection of large and complex structures, in: *2020 IEEE/RSJ International Conference on Intelligent Robots and Systems (IROS)*, IEEE, 2020, pp. 1480–1486.
- [29] G. Mathew, I. Mezić, Metrics for ergodicity and design of ergodic dynamics for multi-agent systems, *Physica D: Nonlinear Phenomena* 240 (4–5) (2011) 432–442.
- [30] P. Virtanen, R. Gommers, T. E. Oliphant, M. Haberland, T. Reddy,

- D. Cournapeau, E. Burovski, P. Peterson, W. Weckesser, J. Bright, S. J. van der Walt, M. Brett, J. Wilson, K. J. Millman, N. Mayorov, A. R. J. Nelson, E. Jones, R. Kern, E. Larson, C. J. Carey, Í. Polat, Y. Feng, E. W. Moore, J. VanderPlas, D. Laxalde, J. Perktold, R. Cimrman, I. Henriksen, E. A. Quintero, C. R. Harris, A. M. Archibald, A. H. Ribeiro, F. Pedregosa, P. van Mulbregt, SciPy 1.0 Contributors, SciPy 1.0: Fundamental Algorithms for Scientific Computing in Python, *Nature Methods* 17 (2020) 261–272. doi:10.1038/s41592-019-0686-2.
- [31] A. R. Conn, N. I. M. Gould, P. L. Toint, *Trust Region Methods*, Society for Industrial and Applied Mathematics, 2000. arXiv: <https://epubs.siam.org/doi/pdf/10.1137/1.9780898719857>, doi:10.1137/1.9780898719857.
URL <https://epubs.siam.org/doi/abs/10.1137/1.9780898719857>
- [32] J. Schöberl, C++11 implementation of finite elements in ngsolve, asc report no. 30/2014 (2014).
- [33] K. K. Poleo, W. J. Crowther, M. Barnes, Estimating the impact of drone-based inspection on the levelised cost of electricity for offshore wind farms, *Results in Engineering* 9 (2021) 100201.
- [34] M. Stokkeland, K. Klausen, T. A. Johansen, Autonomous visual navigation of unmanned aerial vehicle for wind turbine inspection, in: 2015 International Conference on Unmanned Aircraft Systems (ICUAS), IEEE, 2015, pp. 998–1007.
- [35] B. E. Schäfer, D. Picchi, T. Engelhardt, D. Abel, Multicopter unmanned aerial vehicle for automated inspection of wind turbines, in: 2016 24th Mediterranean Conference on Control and Automation (MED), IEEE, 2016, pp. 244–249.